Asian Journal of Chemistry; Vol. 30, No. 2 (2018), 273-279

ASIAN JOURNAL OF CHEMISTRY

https://doi.org/10.14233/ajchem.2018.20888

Synthesis, Characterization and Photocatalysis of γ-Fe_2O_3 Nanoparticles for Degradation of Cibacron Brilliant Yellow 3G-P

HASSAN A. ALSHAMSI* and BATOOL S. HUSSEIN

Department of Chemistry, College of Education, University of Al-Qadisiyah, Post Box 88, Diwaniya, Iraq

*Corresponding author: E-mail: hasanchem70@gmail.com

Received: 23 June 2017; *Accepted*: 30 November 2017; *Published online*: 31 December 2017; AJC-18691

In this study, the maghemite γ-Fe_2O_3 nanoparticles were prepared using a co-precipitation method. The structural, morphological, thermal and its optical properties have been examined using different characterization techniques such as X-ray diffraction, transmission electron microscopy, scanning electron microscopy, energy dispersive spectroscopy, atomic force microscopy, Fourier transform infrared spectrometry, UV/visible spectrophotometer and thermogravimetric analysis. The results of XRD analysis showed the cubic structure of the γ-Fe_2O_3 nanoparticles. Furthermore, the morphology of the γ-Fe_2O_3 nanoparticles was obtained from SEM and AFM. The photocatalytic degradation of Cibacron Brilliant Yellow 3G-P (CB) was studied under visible light using γ-Fe_2O_3 nanoparticles as a photocatalyst. There are many factors, which has an effect on the efficiency of this process. Therefore a study was conducted on the effect of several parameters on γ-Fe_2O_3 like amount of catalyst, concentration of Cibacron Brilliant Yellow 3G-P and pH of solution. The results showed that efficiency of γ-Fe_2O_3 nanoparticles 68 % after 120 min which is more effective on the degradation of Cibacron Brilliant Yellow 3G-P. The photo degraded samples were analyzed by chemical oxygen demand (COD) analysis UV-visible spectrophotometer.

Keywords: γ-Fe_2O_3 nanoparticles, Transmission electron microscopy, Photocatalysis, Cibacron Brilliant, Chemical oxygen demand.

INTRODUCTION

In recent years, iron is create to be more reactive towards water and oxygen in presence of normal air to give common hydrated iron oxides, usually known as rust. The most commonly studied iron oxides nanoparticles such as magnetite Fe_3O_4 and maghemite γ-Fe_2O_3 have been unique magnetic, catalytic, optical, sorption and other properties because of their unique properties that has been utilized in various fields and applications for example magnetic fluids, catalyst, data storage and bionanotechnology [1-4]. The presence of six iron oxides composed of Fe and O: magnetite Fe_3O_4, hematite α-Fe_2O_3, β-Fe_2O_3, maghemite γ-Fe_2O_3, ε-Fe_2O_3 and Wüstite FeO. Iron in most of these compounds, found to be in the trivalent state, but Fe_3O_4 and FeO contain Fe(II). Maghemite, γ-Fe_2O_3 is a red-brown have been found in nature is the ferrimagnetic cubic structure form of ferric oxide then it differs from the opposite spinel structure of magnetite done vacancies on the cation sublattice [5,6]. γ-Fe_2O_3 nanoparticles, is a narrow band gap (2.1 eV) n-type semiconductor [7]. Many synthetic approaches have been advanced to synthesize magnetic iron oxide nanoparticles, including; co-precipitation [8], high-temperature thermal decomposition [9], hydrothermal and solvothermal reaction [10,11], sol-gel reactions [12] and sonochemical reaction [13]. In addition to, the preparation processes and magnetic properties of all iron oxide nanoparticles are connected to their both shape and size have attracted increasing interest may let study of important features of magnetic-ordering externals in magnetic materials with reduction of the dimensions that could cause novelty in many technological applications. Iron oxide nanoparticles have magnetic properties for a strong influence by surface effects, such as the surface area of iron oxide created magnetic materials decreased, their replies to external magnetic field decreased, making it very difficult to regain the adsorbents after treatment has been full [14-16]. The photocatalytic degradation of different toxic organic contaminants is one of the challenging tasks, recently numerous of researches show that the photocatalytic system for iron oxide semiconductor composite can be effectively break through, the bottleneck of the single component semiconductor of oxides that interesting to reprocess from the products, with high reactivity in presence of visible light. The magnetic iron oxide semiconductors can to be an significant magnetic recovery photocatalyst with a glazed future [17-20]. In this paper, the maghemite nanoparticles were synthesized using co-precipitation processes. Various characterizations such as TEM, XRD, FT-IR, AFM, SEM, UV-visible and TGA were measured for identify the prepared γ-Fe_2O_3 nanoparticles. In addition, the photocatalytic activity of

γ-Fe_2O_3 nanoparticles using Cibacron Brilliant Yellow 3G-P (CB) dye studied in presence of visible light, the effect of different parameters on γ-Fe_2O_3 nanoparticles such as dose of γ-Fe_2O_3catalyst, concentration of Cibacron Brilliant Yellow 3G-P and pH also studied on degradation efficiency. The photo degraded samples were analyzed by chemical oxygen demand (COD) analysis.

EXPERIMENTAL

The chemicals used are iron(II) chloride tetrahydrate [$FeCl_2 \cdot 4H_2O$] m.w. = 198.81, iron(III) chloride hexahydrate [$FeCl_3.6H_2O$] m.w. = 270.30 were obtained from Sigma-Aldrich, Cibacron Brilliant Yellow 3G-P dye (99 %), f.w. = 872.97 from Sigma-Aldrich, λ_{max} = 404 nm. The chemical structure of Cibacron Brilliant Yellow 3G-P was shown in (Fig. 1). Absolute ethanol (99.9 %), hydrochloric acid (37 %) and sodium hydroxide were obtained from BDH. All the chemicals were used as received without further purification.

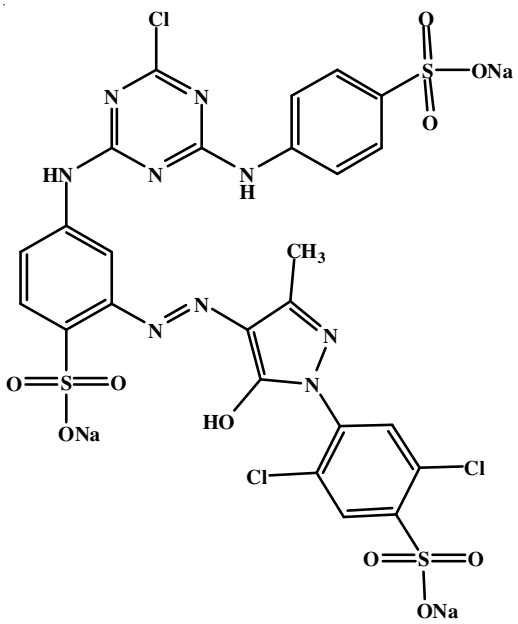

Fig. 1. Structure of Cibacron Brilliant Yellow 3G-P

Preparation of γ-Fe_2O_3 nanoparticle: γ-Fe_2O_3 nanoparticle was prepared by a co-precipitation method, by using of ferric and ferrous ions in alkaline medium [21]. Firstly, powder of 3.25 g $FeCl_3 \cdot 6H_2O$ and $FeCl_2 \cdot 4H_2O$ with molar ratio of Fe^{2+}/Fe^{3+} = 0.5 were dissolving in aqueous solution (60 mL) of hydrochloric acid (50 mL of deionized water added to 10 mL of 1 M HCl) to forming of aqueous solution contain of Fe ions. Then, 100 mL of 1 M of NaOH solution was added drop wise under vigorous stirring for 2 h. Afterward all the Fe ions solution was added, the reaction mixture was stirred additional to prevent coagulation of nanoparticles. After the suspen-sion solution was centrifuged at 3500 rpm, then precipitate was washed repeatedly with deionized water until the pH = 7. Finally the precipitate was dried under normal atmospheric conditions.

Photocatalytic study: The photocatalytic activity of γ-Fe_2O_3 nanoparticles was achieved by degradation of Cibacron Brilliant Yellow 3G-P solution. All the tests were approved under visible light from Xenon lamp 400 W, 40E, Osram. 100 mg of γ-Fe_2O_3catalyst was added to (50 mg/100 mL) Cibacron Brilliant Yellow 3G-P solution then taken and stirred for 120 min in dark to let the physical adsorption of Cibacron Brilliant Yellow 3G-P molecules on the surface of catalyst. Also, this experimental setup was then putted in visible light under stirring for 120 min. The effect of different parameters studied on γ-Fe_2O_3 nanoparticles such as amount of catalyst, concentration of Cibacron Brilliant Yellow 3G-P and pH on degradation efficiency, the pH of the Cibacron Brilliant Yellow 3G-P solution was methodically adjusted through adding 0.1 M NaOH or HCl. The pH meter used for measured pH value of the solutions at room temperature. 5 mL of the samples were taken and centrifuged for 5 min at the rate of 3500 rpm to remove the suspended of γ-Fe_2O_3 catalyst. The Cibacron Brilliant Yellow 3G-P concentration was determined by UV-visible spectrophotometer from the absorption spectra of all the Cibacron Brilliant Yellow 3G-P degradation samples at λ_{max} = 404 nm (Fig. 2) calibration curve of Cibacron Brilliant Yellow 3G-P. The percentage of Cibacron Brilliant Yellow 3G-P degradation was calculated by equation:

$$\text{Degradation (\%)} = \frac{A_o - A_t}{A_o} \times 100 \quad (1)$$

where, A_o is the initial Cibacron Brilliant Yellow 3G-P absorbance; A_t is the absorbance of Cibacron Brilliant Yellow 3G-P at time (t). Samples of Cibacron Brilliant Yellow 3G-P were tested with thermo low-range (0-150) ppm COD test reagent in a TR 300 COD Thermoreactor.

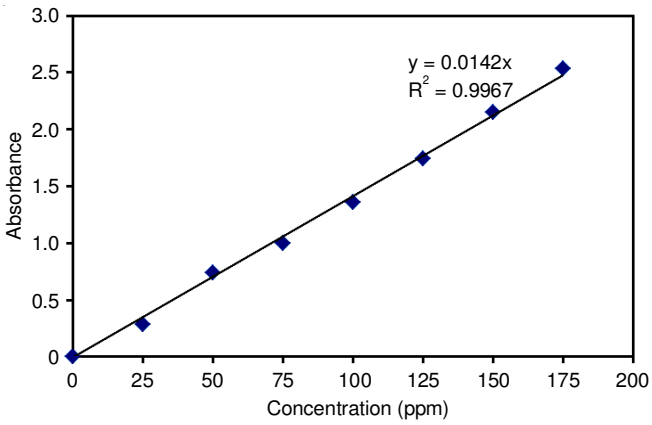

Fig. 2. Calibration curve of Cibacron Brilliant Yellow 3G-P

Characterization of γ-Fe_2O_3 nanoparticles: The crystalline phase of γ-Fe_2O_3 nanoparticles were determined using (XRD-6000, Shimadzu-Japan) with CuK_α radiation (0.15406 nm), the XRD pattern was performed from (20-80)°. Scanning electron microscope (SEM) analysis was approved on nanostructures using Tescan, Vega 3 (Czech) electron microscope with accelerating voltage of 25 kV. The roughness of the surface was recorded by angstrom AFM (SPM-AA3000, USA). The functional groups of nanostructures determined by using FTIR (Shimadzu FTIR 8400s, Japan) analysis in the range 400-4000 cm^{-1} using KBr disc. Thermal stability of γ-Fe_2O_3 nanoparticles was recorded using thermogravimetric Netzsch analyzer (TG 209 F1, Germany) in the temperature range of 10-700 ºC. UV-

visible spectrophotometer (UV-1650, Shimadzu, Japan) was used to determine the spectra of prepared nanoparticles in range from (200-800) nm. The optical band gap E_g was projected from the UV-Vis-NIR diffuse reflectance spectro-scopic (UV-Vis-NIR DRS) determined in a wavelength range from (300-1100) nm with JASCO V-570 spectrophotometer.

RESULTS AND DISCUSSION

X-ray diffraction: Fig. 3 shows the XRD patterns of the prepared γ-Fe_2O_3 nanoparticles. The peaks related with γ-Fe_2O_3 nanoparticles were also detected face-centered cubic structure of γ-Fe_2O_3 nanoparticles which agreed with (JCPDS card no.: 39-1346) accumulated maghemite [22], six peaks appeared at 2θ = 30.42°, 35.80°, 43.49°, 53.90°, 57.48° and 63.10° which correspond to shows the reflections of (220), (311), (400), (422), (511) and (440) which correspond to the cubic structure of γ-Fe_2O_3. No additional impurity peak was noticed in XRD pattern of the prepared sample. The resulted γ-Fe_2O_3 catalysts have a cubic crystal in morphology. Scherrer's formula is used to calculate the particle size using the (311) peak, which was found to be ~ 25.36 nm [23].

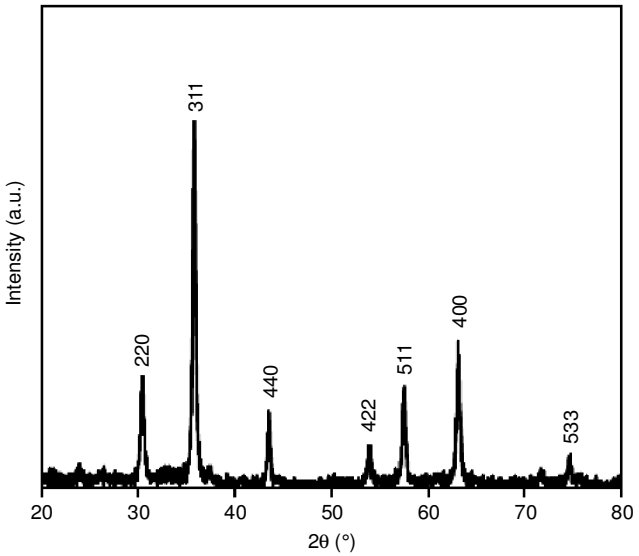

Fig. 3. XRD pattern of γ-Fe_2O_3 nanoparticles prepared

FT-IR analysis: FT-IR measurements have been carried out using KBr pellets method to confirm the formation of crystalline γ-Fe_2O_3 nanoparticles and to identify the presence of any adsorbed species onto the crystal surface. The FTIR spectra of the γ-Fe_2O_3 nanoparticles shows in Fig. 4. The absorption bands between 3741 and 3425 cm^{-1} correspond for both stretching modes surface hydroxyl groups (OH) and the water adsorbed at the surface of γ-Fe_2O_3. The absorption bands present at 1650 and 1535 cm^{-1} correspond to C=O and C-H bonds respectively [24]. The absorption bands at 700-600 and 1172-864 cm^{-1} were identified as CH_3 bending models and the bands at 1442 cm^{-1} is identified as carboxylate stretches. The absorbance peak observed in the spectra The FT-IR spectrum shows the bands from 640 and 570 cm^{-1} due to maghemite vibrations indicates the presence of Fe–O stretching bond range. A last node on these spectra is the presence CO_2 peak around 2352 cm^{-1}, which is a common impurity in IR spectra [25].

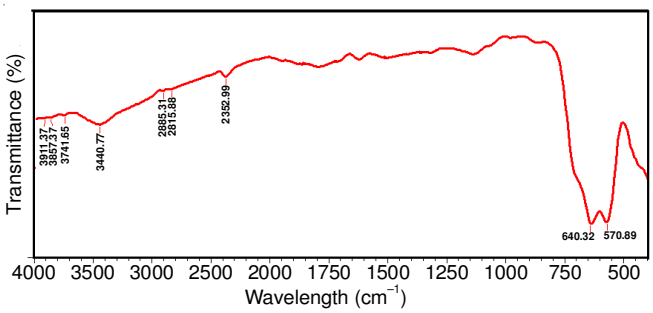

Fig. 4. FTIR spectrum of γ-Fe_2O_3 nanoparticles

Atomic force microscopy analysis: Atomic force microscopy (AFM) was also used to investigate the surface morphology and roughness of γ-Fe_2O_3 nanoparticles. Fig. 5 shows two dimensional (2D), three dimensional (3D) AFM images and particles size distribution of the γ-Fe_2O_3 nanoparticles scanned over a surface area of 1 μm × 1 μm using tapping mode. The AFM image of γ-Fe_2O_3 shows high uniform distribution for particles. The statistical roughness analysis of γ-Fe_2O_3 (CSPM) shows that the obtained roughness average is 0.875 nm, surface skewness is -0.127, root mean square roughness is 1.03 nm and the surface kurtosis is equal to 2.12. The results show that the surface of γ-Fe_2O_3 nanoparticles is bumpy and the valleys are more than the peaks of surface [26]. The size distribution of nanoparticles is shown in Fig. 5c.

SEM analysis: The SEM images (Fig. 6) of the γ-Fe_2O_3 nanoparticles illustrated that the particles are quasi cubic in nature and less agglomerated and they show well-distributed crystallites with average diameter of 25 nm [27]. Also EDS spectrum of γ-Fe_2O_3 nanoparticles shown in Fig. 6B indicated the presence of Fe and O and their high purity. The result is reliable with the results of FT-IR and XRD analyses of the sample prepared.

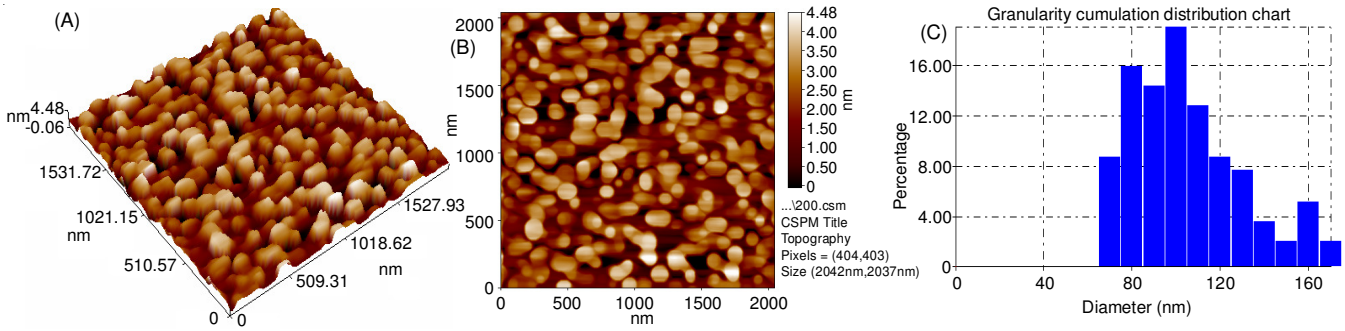

Fig. 5. AFM images of γ-Fe_2O_3 nanoparticles prepared: (A) 3D image, (B) 2D image and (C) particles size distribution

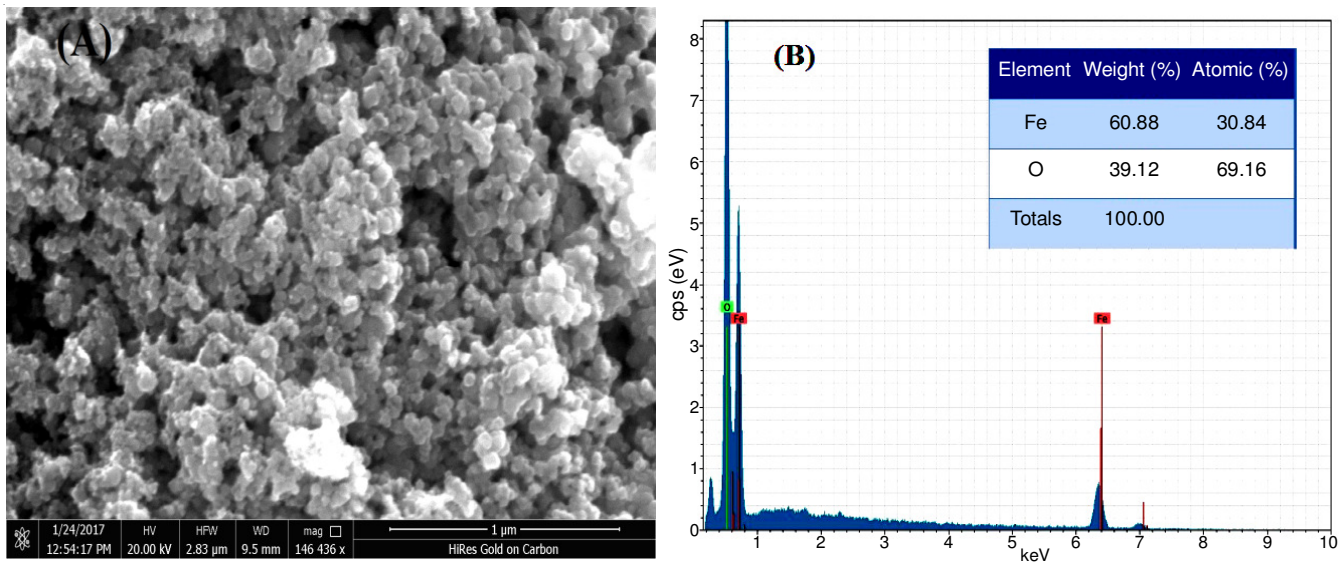

Fig. 6. (A) SEM image of γ-Fe_2O_3 nanoparticles and (B) EDS

Transmission electron microscopic analysis: The crystalline, distribution and the particles size of γ-Fe_2O_3 nanoparticles were shown in TEM image (Fig. 7). TEM image of γ-Fe_2O_3 shows the regular cubic structure with diverse particle size. The small particle size of γ-Fe_2O_3 is approximately equal to 20 ± 35 nm. The less aggregation is shown in TEM image, which was due to the sintering of γ-Fe_2O_3 crystals occurred during the calcination stage.

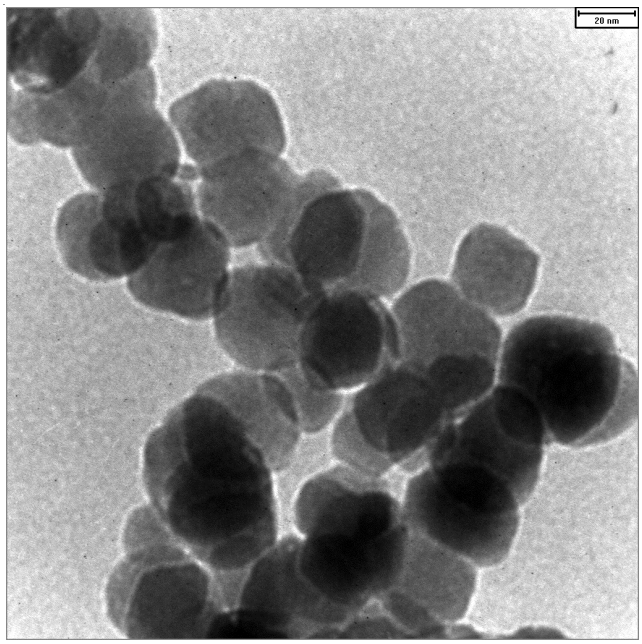

Fig. 7. TEM image of γ-Fe_2O_3 nanoparticles

UV-visible analysis: The optical absorption spectrum and feature of the γ-Fe_2O_3 nanoparticles was observed in Fig. 8 within the range of wavelengths (300-1100 nm). The absorption peak is about 592 nm and the band gap energy of γ-Fe_2O_3 nanoparticles (2.19 eV) was calculated based on the absorption spectrum of the sample using the following equation:

$$E_{bg} = 1240/\lambda_g \quad (2)$$

where, E_{bg} is the band gap energy of γ-Fe_2O_3 photocatalyst, λ_g is the wavelength (nm) used as the absorption edge. In a word, the as-obtained cubic γ-Fe_2O_3 nanoparticles were extended for different potential application in photodegradating of pollutants due to be activated in presence visible light [4]. The band gap calculated by Tauc's plot relationship is expressed as follows:

$$(\alpha h\nu)^{1/n} = C(h\nu - E_g) \quad (3)$$

where α is the absorption coefficient, ν is frequency (ν = c/λ, h is Plancks constant, λ is the wavelength, c light speed,). n = ½ and 2 for indirect and direct optical band gap, respectively. C is proportionality constant and E_g is band gap [28].

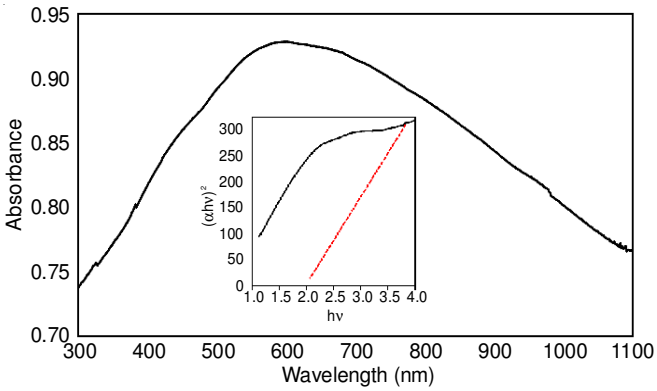

Fig. 8. UV-visible absorbance spectrum and Taucs plot of the γ-Fe_2O_3 nanoparticles

Thermogravimetric analysis of γ-Fe_2O_3 nanoparticles: The relative weight loss of the γ-Fe_2O_3 precursor was studied by thermogravimetric analysis and DSC analysis at inert atmosphere of nitrogen at 10 to 700 °C (Fig. 9). The TGA curve of γ-Fe_2O_3 have a 1 % weight loss in range 360 to 690.9 °C, which indicating to highly purity and high thermal stability of γ-Fe_2O_3 nanoparticles without any loss of organic or water which is adsorbed on the surface of the material. The DSC curve for pure γ-Fe_2O_3 nanoparticles shows an endothermic peak at 637.5 °C, which is attributed to the removal of organic content adsorbed on the surface of γ-Fe_2O_3 nanoparticles.

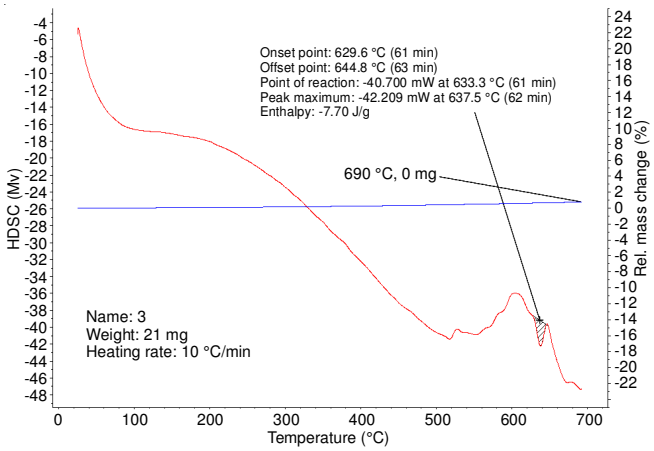

Fig. 9. TGA and DSC of γ-Fe_2O_3 of nanoparticles

Photocatalytic activity of γ-Fe_2O_3 nanoparticles: The photocatalytic activity of γ-Fe_2O_3 nanoparticles for photo-degradation of Cibacron Brilliant Yellow 3G-P was investigated under visible light irradiation. Fig. 10 shows the UV-visible spectrum of Cibacron Brilliant Yellow 3G-P in presence of catalyst with different time, Also the kinetic can often follows pseudo-first-order kinetics, which be represented in Fig. 11 as follows [29]:

$$\ln (C_0/C_t) = kt \quad (3)$$

where C_0 is the initial concentration, C_t concentration Cibacron Brilliant Yellow 3G-P solution at different time and k was the rate constant. The rate constants for Cibacron Brilliant Yellow 3G-P using γ-Fe_2O_3 as photocatalyst; 9.48×10^{-3} min^{-1}. The apparent rate constants γ-Fe_2O_3 having a low band gap energy, so we study effect of concentration of catalyst and Cibacron Brilliant Yellow 3G-P in addition to pH solution. Xenon lamp of 400 W, 40 E, Osram, which emit a continuous spectrum of light in between 400-800 nm was used as a visible light source [27].

Effect of γ-Fe_2O_3 dose: The effect of γ-Fe_2O_3 catalyst dose on photodegradation efficiency was studied by variable the catalyst dose in the range 50-150 mg of γ-Fe_2O_3 with constant concentration of dye 50 ppm as shown in Fig. 12. It is seen that maximum colour removal were 68 % at 100 mg of γ-Fe_2O_3.

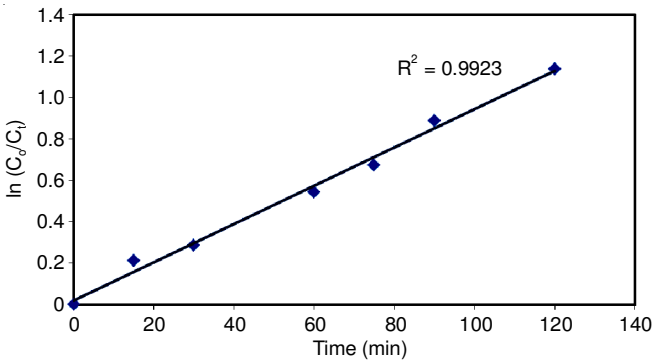

Fig. 11. Plot of ln (C_o/C_t) *versus* time for photocatalytic degradation of Cibacron Brilliant Yellow 3G-P using (γ-Fe_2O_3 = 100 mg, dye cncentration: 50 ppm, pH = 5.1) under visible irradiation

The colour removal increased with increase in the γ-Fe_2O_3 catalyst dose but the degradation efficiency decreases after a certain concentration, this because of in light penetration damage with increasing catalyst dose with increasing γ-Fe_2O_3 catalyst dose the turbidity of the solution increase thus blocking the light and producing scattering [30]. As the γ-Fe_2O_3 doseincreases from 50 to 150 mg, the percentage colour removal increases from 47 to 63 %.

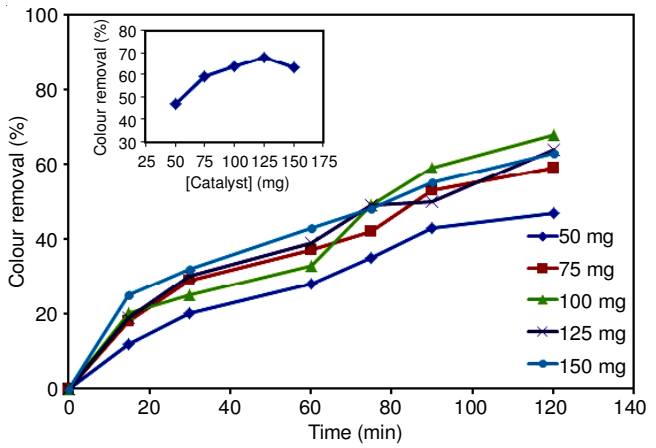

Fig. 12. Effect of γ-Fe_2O_3 dose on colour removal efficiency at 298 K (dye cncentration: 50 ppm, pH = 5.1)

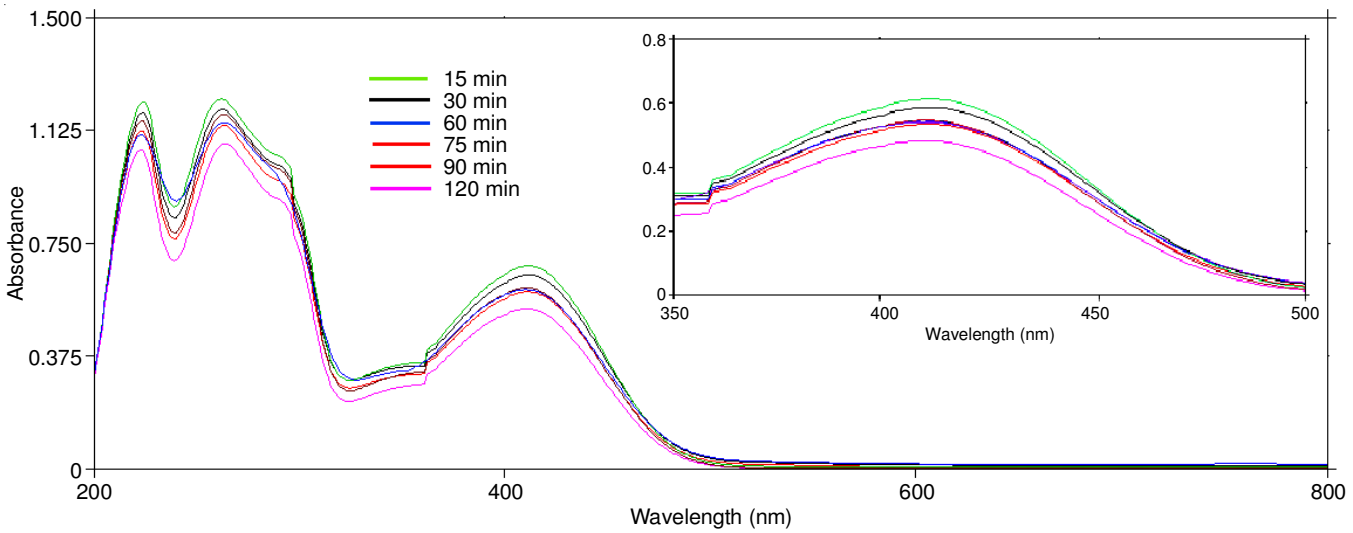

Fig. 10. UV-visible absorption spectrum of dye at 298 K using γ-Fe_2O_3 nanoparticle within different time (catalyst dose: 100 mg/100 mL, Cibacron Brilliant Yellow 3G-P: 50 ppm, 120 min)

Effect of initial dye concentration: The effect of initial concentration of Cibacron Brilliant Yellow 3G-P on photocatalytic activity was studied by changing the initial dye concentration from 25-125 ppm under visible light. The percentage of colour removal efficiency is dependent on the initial Cibacron Brilliant Yellow 3G-P concentration (Fig. 13). The dye degradation efficiency decreases as the Cibacron Brilliant Yellow 3G-P concentration increased. This can be credited to the number of hydroxyl radicals, which remains constant as the γ-Fe_2O_3 catalyst dose 100 mg was kept constant. Maximum dye degradation was observed at 50 ppm. As the Cibacron Brilliant Yellow 3G-P concentration increased the degradation efficiency decreased [31].

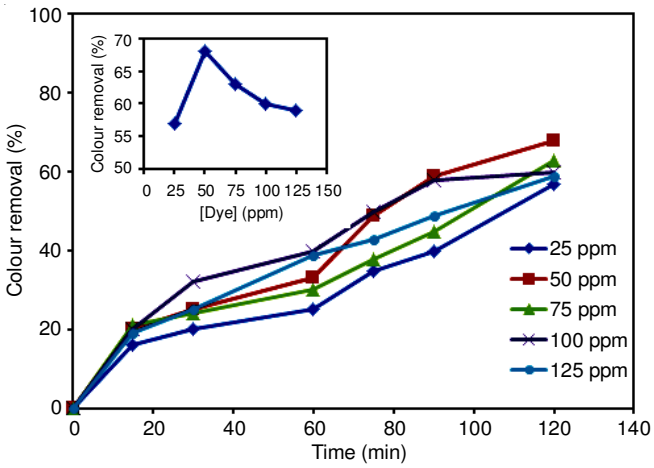

Fig. 13. Effect of initial dye concentration on the colour removal efficiency at 298k (γ-Fe_2O_3 dose: 100 mg, pH = 5.1)

Effect of pH: The effect of pH on the photocatalytic degradation of Cibacron Brilliant Yellow 3G-P were studied by variable the pH of the dye solution 2, 4, 6, 8 and 10 using NaOH or HCl for adjusted the pH of solutions, (Fig. 14) show that pH have a significant effect on the colour removal efficiency. Accor-dingly the plots of percentage degradation as a function of irradiation time (Fig. 14) indicates that the efficiency of photodegradation of the Cibacron Brilliant Yellow 3G-P 68 % at pH solution = 6. The effect of pH value was due to surface charge of the γ-Fe_2O_3 catalyst and the charge on Cibacron Brilliant Yellow 3G-P molecules, such that as the solution becomes more basic at higher pH, the photocatalytic degradation efficiency of the catalyst tends to decrease owing to the development of negative charge on the γ-Fe_2O_3 catalyst surface, which induces repulsion on the negatively charged dye molecules. At pH 10, 46 % dye degradation is observed in 120 min and 68 % at pH 6 dye degradation is observed in 120 min [32,33].

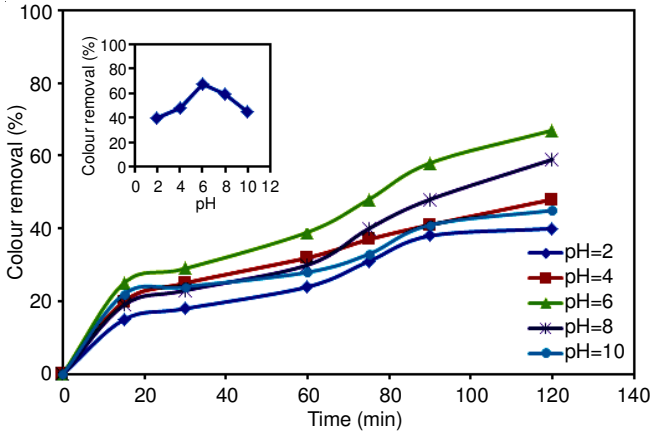

Fig. 14. Effect of different pH value on the colour removal efficiency at 25 °C (dye concentration: 50 ppm, γ-Fe_2O_3 dose: 100 mg, pH = 5.1)

Effect of temperature: Temperature has been an important role in the photocatalytic process, which directly effects on the degradation of Cibacron Brilliant Yellow 3G-P process. Fig. 15 shows that when the solution temperature increases, the colour removal efficiency of Cibacron Brilliant Yellow 3G-P increases when the other experimental conditions stable (50 ppm dye concentration and γ-Fe_2O_3 100 mg) concentration in 50 mL of dye solution), where the dissociation of the dye was studied at three different temperature levels of 293, 298, 303 and 308 K was found at 308 K. Arrhenius equation was used to clarify the relationship between rate consistency and its temperature:

$$\ln k = \ln A - E_a/RT \quad (5)$$

where, k: is rate constant, A: frequency factor, R: gas constant, T: temperature. Fig. 16 shows this effect.

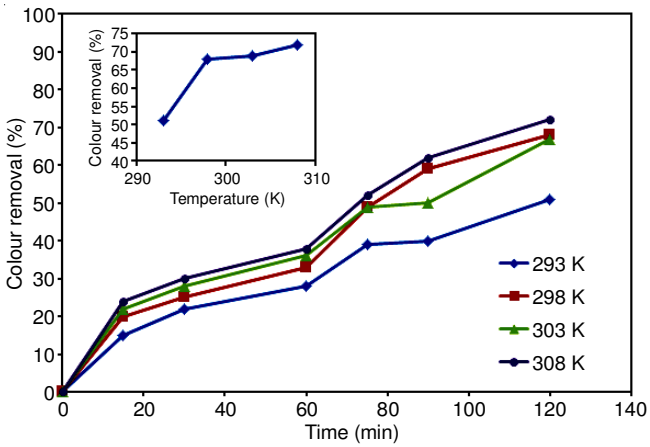

Fig. 15. Effect of temperature on the colour removal efficiency at (dye concentration: 50 ppm, γ-Fe_2O_3 dose: 100 mg and pH = 5.1)

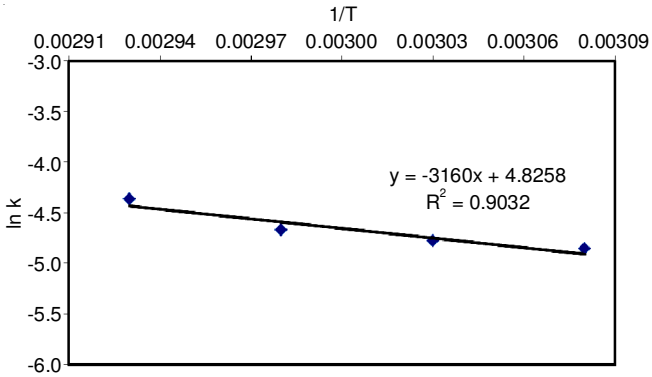

Fig. 16. Arrhenius equation (dye concentration: 50 ppm, γ-Fe_2O_3 dose: 100 mg and pH = 5.1)

Chemical oxygen demand (COD) analysis: The mineralization of Cibacron Brilliant Yellow 3G-P is improved by measuring the COD values at different times of irradiation under enhanced conditions. The percentage of COD removal is 33 %

after 120 min, the results indicates that the almost complete mineralization of Cibacron Brilliant Yellow 3G-P molecules compare with colour removal under visible light is observed was 68 % after 120 min as shown in Fig. 17.

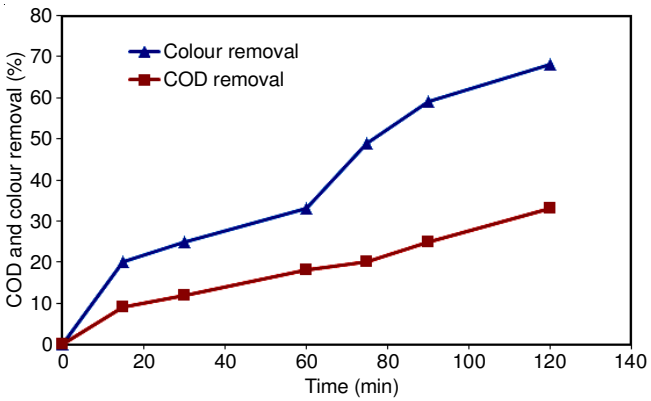

Fig. 17. Colour removal and COD removal of degradation of Cibacron Brilliant Yellow 3G-P concentration: 50 ppm, γ-Fe_2O_3 dose: 100 mg at pH = 5.1 and T = 298 K

Conclusion

In summary, γ-Fe_2O_3 nanoparticles were successfully prepared by co-precipitation method. The prepared nanoparticles were characterized in detail in terms of their structural, morphological, thermal and optical properties. SEM morphology studies confirmed that the γ-Fe_2O_3 nanoparticles are developed in well-crystallinity and cubic crystal shape. The average particles size of γ-Fe_2O_3 nanoparticles was 25 nm as shown in XRD. TEM image shown the particle at 20 ± 35 nm and cubic shape with less agglomerate also, γ-Fe_2O_3 nanoparticles exhibited better photodegradation ability of Cibacron Brilliant Yellow 3G-P. It was observed that the photocatalytic degradation efficiency was enhanced with increasing the amount of γ-Fe_2O_3 and maximum photodegradation was 68 % in presence of 100 mg of the photocatalyst through 120 min. Therefore, γ-Fe_2O_3 nanoparticles can be potentially applied in removing organic dyes from wastewater.

REFERENCES

1. S. Kubickova, D. Niznansky, M. Morales Herrero, G. Salas and J. Vejpravova, *Appl. Phys. Lett.*, **104**, 223105 (2014); https://doi.org/10.1063/1.4881331.
2. H. Shokrollahi, *J. Magn. Magn. Mater.*, **426**, 74 (2017); https://doi.org/10.1016/j.jmmm.2016.11.033.
3. W. Wu, X. Xiao, S. Zhang, T. Peng, J. Zhou, F. Ren and C. Jiang, *Nanoscale Res. Lett.*, **5**, 1474 (2010); https://doi.org/10.1007/s11671-010-9664-4.
4. R.A. Bepari, P. Bharali and B.K. Das, *J. Saudi Chem. Soc.*, **21**, S170 (2017); https://doi.org/10.1016/j.jscs.2013.12.010.
5. S. Saha and A.K. Bhunia, *J. Phys. Sci.*, **17**, 191 (2013).
6. K. Petcharoen and A. Sirivat, *Mater. Sci. Eng. B*, **177**, 421 (2012); https://doi.org/10.1016/j.mseb.2012.01.003.
7. R.A. Bepari, P. Bharali and B.K. Das, *J. Saudi Chem. Soc.*, **21S**, s170 (2017); https://doi.org/10.1016/j.jscs.2013.12.010.
8. M. Aliahmad and N.N. Moghaddam, *Mater. Sci. Pol.*, **31**, 264 (2013); https://doi.org/10.2478/s13536-012-0100-6.
9. S. Capone, M. Manera, A. Taurino, P. Siciliano, R. Rella, S. Luby, M. Benkovicova, P. Siffalovic and E. Majkova, *Langmuir*, **30**, 1190 (2014); https://doi.org/10.1021/la404542u.
10. R. Ianos, E.-A. Tăculescu (Moacă), C. Păcurariu and D. Niznansky, *Mater. Chem. Phys.*, **148**, 705 (2014); https://doi.org/10.1016/j.matchemphys.2014.08.038.
11. T. Daou, G. Pourroy, S. Bégin-Colin, J. Greneche, C. Ulhaq-Bouillet, P. Legaré, P. Bernhardt, C. Leuvrey and G. Rogez, *Chem. Mater.*, **18**, 4399 (2006); https://doi.org/10.1021/cm060805r.
12. J. Hu, G. Chen and I.M. Lo, *Water Res.*, **39**, 4528 (2005); https://doi.org/10.1016/j.watres.2005.05.051.
13. E. Darezereshki, M. Ranjbar and F. Bakhtiari, *J. Alloys Comp.*, **502**, 257 (2010); https://doi.org/10.1016/j.jallcom.2010.04.163.
14. B. Wen, J. Li, Y. Lin, X. Liu, J. Fu, H. Miao and Q. Zhang, *Mater. Chem. Phys.*, **128**, 35 (2011); https://doi.org/10.1016/j.matchemphys.2011.01.012.
15. F. Achouri, S. Corbel, A. Aboulaich, L. Balan, A. Ghrabi, M.B. Said and R. Schneide, *J. Phys. Chem. Solids*, **75**, 1081 (2014); https://doi.org/10.1016/j.jpcs.2014.05.013.
16. Z. Cheng, A.L.K. Tan, Y. Tao, D. Shan, K.E. Ting and X.J. Yin, *Int. J. Photoenergy*, **Article ID 608298** (2012); https://doi.org/10.1155/2012/608298.
17. W. Wu, C.J. Changzhong Jiang and V.A.L. Roy, *Nanoscale*, **7**, 38 (2015); https://doi.org/10.1039/C4NR04244A.
18. W. Wu, Z. Wu, T. Yu, C. Jiang and W.S. Kim, *Sci. Technol. Adv. Mater.*, **16**, 023501 (2015); https://doi.org/10.1088/1468-6996/16/2/023501.
19. V. Patsula, M. Moskvin, S. Dutz and D. Horák, *J. Phys. Chem. Solids*, **88**, 24 (2016); https://doi.org/10.1016/j.jpcs.2015.09.008.
20. C. Okoli, M. Sanchez-Dominguez, M. Boutonnet, S. Järas, C. Civera, C. Solans and G.R. Kuttuva, *Langmuir*, **28**, 8479 (2012); https://doi.org/10.1021/la300599q.
21. L. Jayarathna, A. Bandara, W.J. Ng and R. Weerasooriya, *J. Environ. Health Sci. Eng.*, **13**, 54 (2015); https://doi.org/10.1186/s40201-015-0210-2.
22. W. Wu, X. Xiao, S. Zhang, J. Zhou, L. Fan, F. Ren and C. Jiang, *J. Phys. Chem. C*, **114**, 16092 (2010); https://doi.org/10.1021/jp1010154.
23. P. Saravanan, J.-H. Hsu, D. Sivaprahasam and S.V. Kamat, *J. Magn. Magn. Mater.*, **346**, 175 (2013); https://doi.org/10.1016/j.jmmm.2013.07.023.
24. O. Stefanescu, C. Davidescu and C. Muntean, *Ann. West Univ. Timisoara Series of Chemistry*, **24**, 69 (2015).
25. A. Asfaram, M. Ghaedi, S. Hajati and A. Goudarzi, *Ultrason. Sonochem.*, **32**, 418 (2016); https://doi.org/10.1016/j.ultsonch.2016.04.011.
26. M. Belkhedkar and A. Ubale, *Int. J. Mater. Chem.*, **4**, 109 (2014).
27. C. Liang, H. Liu, J. Zhou, X. Peng and H. Zhang, *J. Chem.*, **Article ID 791829** (2015); https://doi.org/10.1155/2015/791829.
28. S.S. Al-Taweel and H.R. Saud, *J. Chem. Pharm. Res.*, **8**, 620 (2016).
29. L.S.J. Al-Hayder and M.K. Al-Hussainawy, *Int. J. Chemtech Res.*, **9**, 337 (2016).
30. L.K. Mun, A.H. Abdullah, M.Z. Hussein and Z. Zainal, *Sains Malays.*, **43**, 437 (2014).
31. Z. Jia, J. Miao, H.-B. Lu, D. Habibi, W. Zhang and L. Zhang, *J. Taiwan Inst. Chem. Eng.*, **60**, 267 (2016); https://doi.org/10.1016/j.jtice.2015.10.012.
32. M.N. Chong, B. Jin, C.W. Chow and C. Saint, *Water Res.*, **44**, 2997 (2010); https://doi.org/10.1016/j.watres.2010.02.039.
33. L.S.J. Al-Hayder and M.H.J. Al-Juboory, *J. Chem. Pharm. Res.*, **7**, 1138 (2015).